EXTRACTING GEOMETRIC FEATURES OF AORTIC VALVE ANNULUS MOTION FROM DYNAMIC MRI FOR GUIDING INTERVENTIONS

Nikhil V. Navkar[1,2]*, Erol Yeniaras*[2]*, Dipan J. Shah*[3]*, Nikolaos V. Tsekos*[2]*, Zhigang Deng*[1]

[1]Computer Graphics and Interactive Media Lab, and [2]Medical Robotics Lab,
Department of Computer Science, University of Houston, Houston, TX 77004, USA
[3]Methodist DeBakey Heart & Vascular Center, Methodist Hospital, Houston, TX 77030, USA

ABSTRACT

Transcatheter aortic valve implant (TAVI) has emerged as a prominent approach for treating aortic stenosis. Success of such implants depends upon the accurate assessment of the geometric features such as the diameter, center and orientation of the aortic valve annulus (AVA). In this paper, we present a method for extracting these geometric features from magnetic resonance images (MRI). The method is based on finding an optimal fit for a circular ring mimicking AVA in the aortic root. Moreover, the presented approach provides dynamic tracking of the AVA in CINE MR images. This approach can be used for preoperative planning of prosthetic valve implantation, as well as for the emerging MRI guided manual, or with robot-assisted, annuloplasty.

Index Terms— Aortic Valve Annulus, Magnetic Resonance Imaging, Robot-Assisted Cardiac Surgery.

1. INTRODUCTION

Aortic stenosis is the most common valvular heart disease prevalent in the elderly population [1]. Conventional therapy for the treatment of aortic stenosis involves a surgery for replacing the aortic valve. This surgical procedure entails cardiopulmonary bypass that may pose high risks to certain patients [2]. An alternative approach, the transcatheter aortic valve implant (TAVI), has been introduced to overcome the shortcoming of the conventional aortic valve replacement [3]. Success of a minimally-invasive TAVI surgery highly depends upon proper preoperative planning as well as accurate intraoperative placement of the implant. One of the major steps during the preoperative planning is accurate estimation of various AVA geometric features, such as its diameter, center, and orientation. Determination of these AVA geometric features is crucial to deciding the size and type of the prosthesis valve to be used. Deployment of a small prosthesis may lead to prosthesis embolization; whereas, prosthesis with a size larger than the optimum may damage the aortic root or even cause a high-grade atrioventricular block. Thus, accurately estimating AVA geometric features is crucial to the success of TAVI.

Generally, image-based, pre-operative measurement of the AVA geometric features is based on transthoracic echocardiography (TTE), transesophageal echocardiography (TEE), and multi-slice computed tomography (MSCT). Currently, there is no gold standard of using a particular method over other for measuring the AVA size before TAVI [4]. An alternative to ultrasound and x-ray based methods, is MRI for tracking AVA. As compared to other imaging modalities for estimating AVA, MRI offers certain features beneficial to both preoperative planning and intraoperative guidance: it is non-invasive (unlike TEE that requires access via the esophagus), does not involve ionizing radiation (unlike MSCT), and provides superior soft tissue contrast with a large field-of-view (unlike TTE). It should be noted that MRI also has certain limitations, including: offering limited access to the patient inside standard cylindrical MR scanners, not as fast as ultrasound imaging, and entailing high and rapidly switching magnetic field gradients that impose restrictions on the employed interventional tools. However, the aforementioned benefits have led numerous research efforts on the development of MRI-guided TAVI procedures [5, 6, 7].

In addition to measuring AVA geometric features preoperatively, MRI can also be used intraoperatively during TAVI to guide a prosthesis valve [5]. Minimally invasive image-guided robot-assisted systems have been proposed for transapical aortic valve replacement [6]. For these robotic systems, apart from the AVA diameter, it is also important to understand how the AVA moves with respect to its surrounding tissue during a cardiac cycle. The AVA center acts as a target for the robot's end effector, and the AVA orientation specifies the direction along which the prosthesis valve can be deployed.

In this work, we propose a method that determines various geometric features (including diameter, center and orientation) of an AVA and also helps in the preoperative visualiza-

This work was supported in part by the National Science Foundation award CNS-0932272 and IIS-0914965. Any opinions, findings, and conclusions or recommendations expressed in this material are those of the authors and do not necessarily reflect the views of the funding agencies.

We would like to thanks Karen Chin from Methodist Hospital, Houston, for helping us to collect MR image data sets.

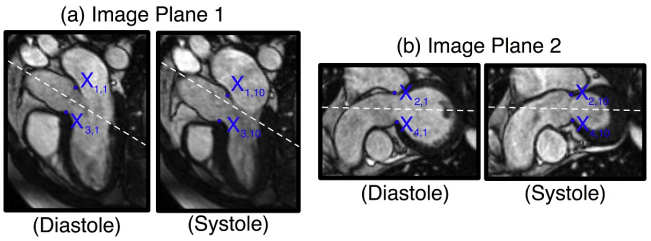

Fig. 1: Representative examples of the two imaging planes used by the proposed method for the extraction of the geometric features of the AVA. Only the diastolic and systolic phases are shown (out of 20 frames over the cardiac cycle). (a) This long axis plane is used to calculate points $\mathbf{X_{1,t}}$ and $\mathbf{X_{3,t}}$ (shown in blue color). The white dotted line on image plane 1 shows the projection of imaging plane 2 on it. (b) The second imaging plane, a short axis view, is used to calculate points $\mathbf{X_{2,t}}$ and $\mathbf{X_{4,t}}$.

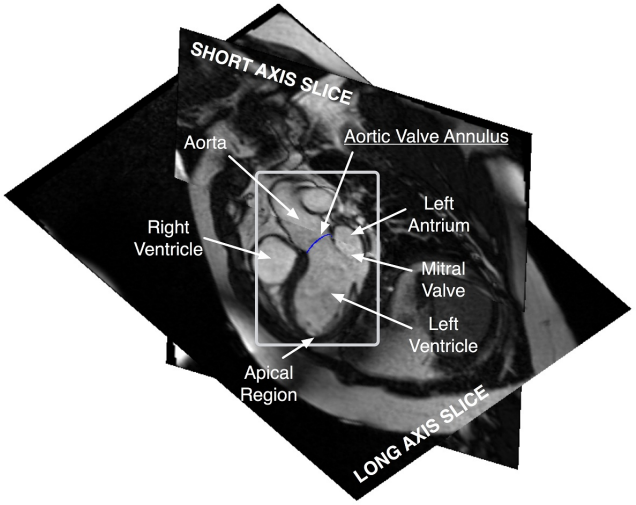

Fig. 2: Aortic valve annulus position with respect to short and long axis slices for a single time instant. The positioning of annulus for complete cardiac cycle (within the marked rectangular area) is shown in Figure 3.

tion and tracking of its motion relative to the other anatomical structures inside the heart. The latter property is pursued in view of the emerging MRI-guided aortic valve implantation with robotic assistance [5] or without it [6].

2. METHODOLOGY

The proposed approach consists of three computational steps. First, certain points corresponding to an AVA are selected on dynamic cardiac images. Second, an initial approximation on the AVA is calculated in the initialization phase. Finally, the approximate values are further optimized. The follow-up sections describe each step in details.

For the sake of a clear explanation, we first introduce some terms: At a time instance t during the cardiac cycle, the AVA can be described as a circular ring with a radius R_t centered at a point $\mathbf{C_t}$, where $\mathbf{C_t} \in R^3$ (Although pathological studies shows AVA as semilunar crown-like ring, for the purpose of TAVI it is treated as a circular shaped ring). These geometric entities are relative to the MR scanner coordinate system. Furthermore, the orientation of this ring in the three-dimensional (3D) space can be defined by an axis described by a vector $\mathbf{N_t}$ that passes through the center $\mathbf{C_t}$ and is orthogonal to the plane on which the ring lies.

2.1. Aortic Valve Annulus Point Selection

The motion of an AVA is not restricted on a single plane. Therefore, it is not possible to accurately analyze the AVA features with the aid of a single two-dimensional (2D) image with fixed orientation. In order to locate the dynamic AVA, two imaging planes are used. The first plane is a long axis view of left ventricle (LV) depicting the apical region of the heart, the mitral valve and the aortic valve (Fig. 1(a) shows a representative example of such plane marked as Plane 1). The second plane is a short axis view prescribed to include the aorta, the aortic valve and left ventricle (Fig. 1(b) shows such a plane marked Plane 2). In this proof-of-concept work we use CINE MR images with a time resolution of 60 msec. Since the datasets were collected during breath hold and were ECG triggered, they can be straightforwardly registered in a four-dimensional (4D) space. Note that they share the same inherent coordinate system of the MRI.

Two points: $(\mathbf{X_{1,t}}, \mathbf{X_{3,t}})$ and $(\mathbf{X_{2,t}}, \mathbf{X_{4,t}})$, are marked for every time frame on the first and the second imaging plane, respectively. These points are represented in 3D space as $\mathbf{X_{i,t}} = [\mathbf{x_{i,t}}, \mathbf{y_{i,t}}, \mathbf{z_{i,t}}]^\mathbf{T}$ with respect to the MR scanner coordinate system. These points can be marked for different time frames either manually or with automated algorithms (e.g. [8, 9]). The points are marked on an image where the aortic leaflet is attached to the aortic wall (shown in Fig. 1). The four points are then denoted in the form of a vector $\mathbf{X_t} = [\mathbf{X_{1,t}}, \mathbf{X_{2,t}}, \mathbf{X_{3,t}}, \mathbf{X_{4,t}}]$.

2.2. Aortic Valve Annulus Initialization

The initialization phase gives an approximation of the values of $\mathbf{C_t}$, R_t, and $\mathbf{N_t}$ for an AVA. The Singular Value Decomposition (SVD) technique is applied on the vector $\mathbf{X_t}$ to factorize it into unitary matrices $\mathbf{U_t}$ and $\mathbf{V_t}$, and a diagonal matrix $\mathbf{D_t}$:

$$\mathbf{X_t} = \mathbf{U_t D_t V_t}^\mathbf{T} \tag{1}$$

Since the four points $\{\mathbf{X_{i,t}}\}_{i=1}^{4}$ almost lie on a plane, the vector $\mathbf{X_t}$ that represents the points in the MR scanner coordinate system is transformed to a vector $\tilde{\mathbf{X}}_\mathbf{t} = [\tilde{\mathbf{X}}_{\mathbf{1,t}}, \tilde{\mathbf{X}}_{\mathbf{2,t}}, \tilde{\mathbf{X}}_{\mathbf{3,t}}, \tilde{\mathbf{X}}_{\mathbf{4,t}}]$ in the SVD space by applying following transformation:

$$\tilde{\mathbf{X}}_\mathbf{t} = \mathbf{U_t}^\mathbf{T} \mathbf{X_t} \tag{2}$$

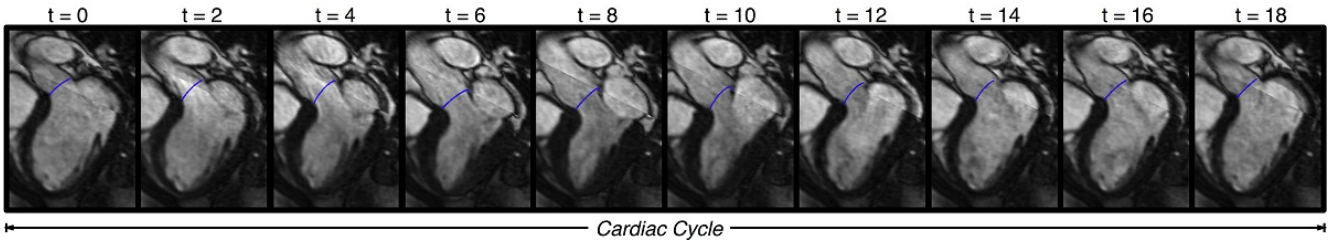

Fig. 3: Representative results of AVA tracking with the proposed method showing 10 (out of 20) frames at selected instances over a cardiac cycle. The blue curve represents the aortic valve annulus for different time intervals. The cardiac cycle is discretized into 20 time frames. Only 10 frames at regular time interval (t=$\{2i : i$ is from 0 to $9\}$) are shown.

Then, we fit a circle in 2D space to the transformed points $\{\tilde{\mathbf{X}}_{\mathbf{i,t}}\}_{i=1}^{4}$ in the vector $\tilde{\mathbf{X}}_{\mathbf{t}}$ using the fitting technique proposed by Taubin [10]. In this way, we will obtain the estimated center $\tilde{\mathbf{C}}_{\mathbf{t}}$ and radius R_t. Note that the z coordinate of the transformed points is ignored in this process.

Finally, an inverse transformation is applied to compute the corresponding estimated center in the MR coordinate system:

$$\mathbf{C_t} = \mathbf{U_t}\tilde{\mathbf{C}}_{\mathbf{t}} \tag{3}$$

Similarly, the direction vector $\mathbf{N_t}$ representing the orientation of the AVA in 3D space is calculated as:

$$\tilde{\mathbf{N}}_{\mathbf{t}} = (\tilde{\mathbf{X}}_{\mathbf{2,t}} - \tilde{\mathbf{X}}_{\mathbf{1,t}}) \times (\tilde{\mathbf{X}}_{\mathbf{3,t}} - \tilde{\mathbf{X}}_{\mathbf{1,t}}) \tag{4}$$

$$\mathbf{N_t} = \mathbf{U_t}\tilde{\mathbf{N}}_{\mathbf{t}} \tag{5}$$

2.3. Aortic Valve Annulus Optimization

To optimize the AVA features, we define an energy function E_t (Eq. 6). Minimizing this energy function further optimizes the values of $\mathbf{C_t}$, R_t, and $\mathbf{N_t}$ for the AVA. For a time instance t, E_t represents the summation of distances between the AVA circumference and the marked points $\mathbf{X_{i,t}}$:

$$E_t = \sum_{i=1}^{4} \left({R_t}^2 + \|\hat{\mathbf{X}}_{\mathbf{i,t}}\|^2 - 2R_t\|\hat{\mathbf{X}}_{\mathbf{i,t}}\| \sin\theta \right)^{\frac{1}{2}} \tag{6}$$

$$\hat{\mathbf{X}}_{\mathbf{i,t}} = \mathbf{X_{i,t}} - \mathbf{C_t} \tag{7}$$

where θ is the angle between the vector $\hat{\mathbf{X}}_{\mathbf{i,t}}$ and $\mathbf{N_t}$.

3. RESULTS

The proposed approach was tested on MR data sets collected from three healthy volunteers. The MRI data sets were collected with true fast imaging, steady state precession (True-FISP) pulse sequence with the acquisition parameters: TR = 2.3 ms, TE = 1.4 ms, α = 80°, slice thickness = 6 mm, and acquisition matrix = 224x256. For a single cardiac cycle, depending upon the MR scanner, 20 to 25 cardiac image samples were captured. In our experimental studies, the t value varies from 1 to 20.

The average AVA diameters of the three subjects were found to be 26.81 mm, 26.25 mm, and 24.56 mm, respectively. Changes in the AVA diameter in a cardiac cycle are shown in Fig. 5. The motion of the AVA is visually analyzed in a 3D space using two oblique MRI planes. Fig. 2 shows the relative position of the AVA with respect to different anatomical structures inside the heart, depicted on a long and short axis view for a single time instant. The complete motion of the AVA for a cardiac cycle is shown in Fig. 3. In the given example, the image plane used for marking the points $(\mathbf{X_{1,t}}, \mathbf{X_{3,t}})$ is the same as that of long axis view slice. However, the imaging plane used for marking point $(\mathbf{X_{2,t}}, \mathbf{X_{4,t}})$ is different from the short axis view shown in Fig. 2 and Fig. 3. The blue curve in Fig. 3 shows that the AVA aligns accurately with the new short axis view. The proposed method also helps to track the motion of an AVA in general. The positions of an AVA relative to each other for different time instances in a cardiac cycle are shown in Fig. 4.

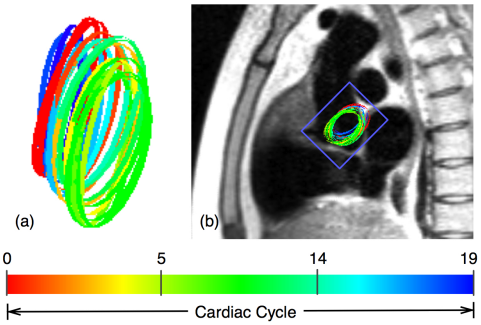

Fig. 4: Composite motion of an aortic valve annulus. (a) The cardiac cycle is color-coded (as shown on the time scale). Each color represents the position of the aortic valve annulus at different instants of the cardiac cycle. All the positions are relative to the MR coordinate system. (b) A dark-blood MR image is used to show the relative position of the aortic valve annulus with respect to heart.

To validate the results for every marker point $\mathbf{X_{i,t}}$ (i = 1 to 4, and t = 0 to 19), we measure the average of the minimum distances between the marker points and the circumference of the AVA (represented by E_{Xi}). Table 1 shows the changes in

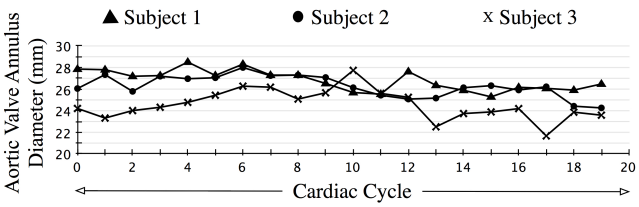

Fig. 5: The measured diameter of the aortic valve annulus in a cardiac cycle extracted from the CINE MR images.

E_{X1}, E_{X2}, E_{X3}, and E_{X4} in a cardiac cycle. As the pixel size of the given images is 1.56 mm x 1.56 mm, we rounded the minimum distances between the marker points and the circumference of the AVA in terms of pixels. For example, if the distance is between 0 and 1.56 mm, it was rounded to 1 pixel. Table 1 shows the percentage of samples for which the error value is measured in terms of pixels.

4. DISCUSSION

The proposed method was investigated on the high contrast CINE MR data. While such MR data are suitable for pre-operative planning, CINE MR is not a true real-time MR sequence suitable for intraoperative analysis. Our future work will investigate the method with real-time MRI. With the help of tissue tracking algorithms [8, 9] and RT-cine MR images, it would allow us to track the motion of the AVA in real-time. This will enable the application of this method for guiding robot-assisted prosthetic valve delivery system for aortic valve replacement under real-time-MRI guidance via transapical approach [5, 6]. The imaging planes used by our method to detect the AVA have the similar orientations to those of RT-MRI planes for guiding the robot's end effector. The proposed method could also be applied for tracking the motion of annulus of right atrioventricular and pulmonary valve by capturing dynamic MR cardiac images at different orientations. However, the mitral valve annulus cannot be tracked with the given technique because of its non-circular shape.

5. CONCLUSIONS

In this paper, we propose a simple yet effective method to quantitatively analyze the motion of the AVA using dynamic cardiac MR images. The method tracks the center, orientation and diameter of the annulus over a cardiac cycle. Compared with other methods, our approach gives a dynamic composite view of AVA motion with respect to other anatomical structures inside the heart. The results visually show that the circular ring representing the AVA found by our approach fits well on any dynamic cardiac MR images depicting aortic valve. The method would be useful, especially in TAVI under MR guidance.

Subject	Error (Pixels)		Average Minimum Distances (mm)			
	≤ 1	1 to 2	E_{X1}	E_{X2}	E_{X3}	E_{X4}
1	78.8%	16.3%	0.25	0.00	1.33	1.48
2	77.5%	12.5%	0.64	2.47	0.25	0.00
3	75.3%	10.4%	1.56	0.10	1.91	1.00

Table 1: Error is measured in term of pixel spacing for the three subjects. Also, the average minimum distances E_{X1}, E_{X2}, E_{X3}, and E_{X4} for the four points: $\mathbf{X_{1,t}}, \mathbf{X_{2,t}}, \mathbf{X_{3,t}}, \mathbf{X_{4,t}}$ are measured.

6. REFERENCES

[1] V.T. Nkomo, J.M. Gardin, T.N. Skelton, J.S. Gottdiener, C.G. Scott, and M.E. Sarano, "Burden of valvular heart diseases: a population-based study," *The Lancet*, vol. 368, pp. 1005 – 1011, 2006.

[2] T.M. Dewey, D. Brown, W.H. Ryan, M.A. Herbert, S.L. Prince, and M.J. Mack, "Reliability of risk algorithms in predicting early and late operative outcomes in high-risk patients undergoing aortic valve replacement.," *J Thorac Cardiovasc Surg*, vol. 135, pp. 180 – 187, 2008.

[3] A. Cribier, H. Eltchaninoff, A. Bash, N. Borenstein, C. Tron, F. Bauer, G. Derumeaux, F. Anselme, F. Laborde, and M. Leon, "Percutaneous transcatheter implantation of an aortic valve prosthesis for calcific aortic stenosis: First human case description.," *Circulation*, vol. 106, pp. 3006 – 3008, 2002.

[4] A. Hutter, A. Opitz, S. Bleiziffer, H. Ruge, I. Hettich, D. Mazzitelli, A. Will, P. Tassani, R. Bauernschmitt, and R. Lange, "Aortic annulus evaluation in transcatheter aortic valve implantation.," *Catheterization and cardiovascular interventions*, 2010.

[5] E.R. McVeigh, M.A. Guttman, R.J. Lederman, M. Li, O. Kocaturk, T. Hunt, S. Kozlov, and K.A. Horvath, "Real-time interactive mri-guided cardiac surgery: Aortic valve replacement using a direct apical approach," *Magnetic Resonance in Medicine*, vol. 56, pp. 958 – 964, 2006.

[6] M. Li, D. Mazilu, and K.A. Horvath, "Robotic system for transapical aortic valve replacement with mri guidance," in *Medical Image Computing and Computer Assisted Intervention (MICCAI 2008)*, 2008, pp. 476 – 484.

[7] K.A. Horvath, M. Li, D. Mazilu, M.A. Guttman, and E.R. McVeigh, "Real-time magnetic resonance imaging guidance for cardiovascular procedures.," *Seminars in thoracic and cardiovascular surgery.*, vol. 19, pp. 330–335, 2007.

[8] M. Dewan, *Image-based Tracking Methods - Applications to Improved Motion Compensation in Cardiac MR and Image-Guided Surgery*, Ph.D. thesis, Johns Hopkins University, Baltimore, Maryland, USA, September 2007.

[9] Y. Zhou, E. Yeniaras, P. Tsiamyrtzis, N. Tsekos, and I. Pavlidis, "Collaborative tracking for mri-guided robotic intervention on the beating heart," in *Medical Image Computing and Computer Assisted Intervention (MICCAI 2010)*, 2010, pp. 351– 358.

[10] G. Taubin, "Estimation of planar curves, surfaces and nonplanar space curves defined by implicit equations, with applications to edge and range image segmentation," *IEEE Trans. Pattern analysis and Machine Intelligence*, vol. 13, pp. 1115–1138, 1991.